J Mater Sci: Mater Med (2011) 22:2019–2028
DOI 10.1007/s10856-011-4390-8

Solvent and melting induced microspheres sintering techniques: a comparative study of morphology and mechanical properties

A. Luciani · V. Guarino · L. Ambrosio · P. A. Netti

Received: 5 May 2011 / Accepted: 4 July 2011 / Published online: 24 July 2011

Abstract In this work we propose a bottom up approach founded on the assembly of building blocks by solvent induced microparticle sintering to realize multifunctional polymer scaffolds with predefined pore dimension and fully percolative pathway, able to include interspersing microdepot for the release of bioactive molecules. The aim of this study was to develop a versatile method of microspheres sintering based on the partial dissolution of the surface of adjacent microparticles and to compare it with melting induced microspheres sintering, just developed in a previous work. The two techniques were compared in terms of morphology, porosity and mechanical properties. The high potential of customizing the sintering process by the proper selection of the sintering techniques as well as microparticles with different features (e.g., material, size, shape, inner porosity) allows obtaining a wide pattern of micro/nanostructures with bio-inspired mechanical response so satisfying all basic requirements of a "smart" scaffold for bone tissue engineering.

A. Luciani (✉) · P. A. Netti
Interdisciplinary Research Centre on Biomaterials (CRIB), University of Naples Federico II, P.le Tecchio 80, Naples 80125, Italy
e-mail: a.luciani@unina.it

A. Luciani · P. A. Netti
Italian Institute of Technology (IIT), University of Naples Federico II, P.le Tecchio 80, Naples 80125, Italy

A. Luciani · V. Guarino · L. Ambrosio
Institute of Composite and Biomedical Materials, National Research Council (IMCB-CNR), P.le Tecchio 80, Naples 80125, Italy

1 Introduction

Nowadays, technologies applied to the biomedicine rely on the ability to control material properties on different length scales. Novel bottom up techniques are being explored as complementary strategies to traditional top down methods for developing a new concept of micro/nano-structured materials with desired features from fundamental elementary units or building blocks. This approach not only requires the full knowledge and control of the individual building block properties, but is also founded on the intimate knowledge of the assembly methods of construction units, moving progressively towards an increasing complexity degree of the material design [1].

In this context, a promising bottom-up strategy for scaffold design involves the assembly of microparticles with predefined properties and structure, which act as building blocks to assemble three-dimensional (3D) complex architecture with defined mechanical strength and spatial–temporal distribution of bioactive molecules. This approach offers the possibility to realize scaffolds that not only meet all the requirements in terms of controlled microstructure, chemical stability and mechanical response necessary to support neo-tissue growth, but also provide a guidance of cell and tissue processes by presenting bioactive agents in a predefined chrono-programmed manner [2]. In recent years several studies concerning the production of porous scaffolds by thermal sintering microspheres have been reported [3, 4]. As soon as a microsphere based approach for the production of tissue engineering 3D scaffolds with a porous interconnected structure was

proposed [5], it became evident that the bottom-up approach could overcome some of the limitations presented by the classical scaffold manufacturing. In particular, bottom up approach allows a better control of porosity, interconnectivity and mechanical properties of the resulting scaffold along with the inclusion of micro-depots in a predefined spatial pattern. Indeed, it has been demonstrated that it is possible to reproduce a porous 3D structure with the morpho-functional aspect of the cancellous bone [6], with a porosity (30 Vol%) that may be considered biomimetically equivalent to that of trabecular bone [7] and with mechanical properties equivalent to that of cancellous bone [8].

In our previous work we had shown the possibility to include small protein-loaded microparticles within the sintered scaffolds to perform a sustained delivery of a model-protein (i.e., BSA). It has been shown that loaded microspheres act as local chrono-programmed point source of bioactive signals, allowing to include the control of their spatial–temporal presentation in a scaffold with a predefined size and extension of the porosity and mechanical properties [9]. However, melting induced microspheres sintering (MIMS) poses some limitations when treating with thermolabile bioactive molecules which tend to denature with temperature. Solvent induced microspheres sintering (SIMS) is a versatile method of sintering polymeric microspheres under mild temperature conditions providing the sintering through the partial dissolution of the microsphere surface with a properly selected solvent mixture [10, 11]. Another methods to process bottom up scaffold is based on the use of modified selective laser sintering (SLS) machine to sinter bio-nanocomposite microspheres, consisting of carbonated hydroxyapatite (CHAp) nanospheres within a poly(L-lactide) (PLLA) matrix [12]. More recently, scaffolds that can sequentially deliver IGF-I and TGF-β1 were fabricated by chemical compaction of IGF-I and TGF-β1 loaded microspheres [13, 14].

Along these lines, here we propose a bottom up approach founded on the assembly of building blocks by SIMS. Our aim was to find a correct mixture of solvents in order to balance its dissolution power and evaporation kinetic to control the bonding degree among the microspheres. By this strategy, the chemical assembly of large polycaprolactone (PCL) microparticles with diameter from 300 to 630 μm, obtained via single emulsion technique, has been performed by dipping them into an appropriately chosen solvent bath. Moreover, protein-loaded scaffold has been developed by sintering large microparticles together with smaller protein-loaded microparticles, with 50–180 μm size range, obtained by double emulsion technique. A comparative morphological and structural study of porous scaffolds obtained by SIMS and MIMS techniques was assessed to demonstrate the possibility to switch from MIMS to SIMS technique as a function of scaffold porosity and mechanical requirements needed for different applications in bone tissue engineering.

2 Materials and methods

2.1 Materials

Poly(ε-caprolactone) (PCL) (Mw = 65 kDa), polyvinyl alcohol (PVA) (MW: 13–23 kDa, 87–89% hydrolyzed), dichloromethane, chloroform, dioxane and Bovine serum albumin (BSA) were all purchased from Sigma-Aldrich (Italy) and used as received.

2.2 Building blocks: microspheres via single and double emulsion techniques

PCL microspheres were prepared by single emulsion technique, as already described in [9]. Briefly, PCL (24% w/v) was dissolved in 20 ml of dichloromethane and added to an aqueous solution of PVA (0.25% w/v) stirred for 3 h at 400 rpm at room temperature. The organic solvent was extracted from the PCL to obtain solid microspheres. Then, the microspheres were filtered and washed with de-ionized water to remove possible traces of organic solvent. Microspheres were separated selectively into the following size ranges by using commercial sieves (Sieves IG/3-EXP, Retsch, Germany): 300–500 μm; 500–630 μm.

BSA-loaded microspheres were obtained by the double emulsion-solvent evaporation technique, as already described in [15]. Briefly, an aqueous solution of BSA was added drop-wise into 9 ml of a PCL solution in dichloromethane (3% w/v) and emulsified for 30 s using a sonicator (Grant ultrasonic bath XB3, 50–60 Hz, 60 W, UK). The primary emulsion (W/O) was added to 250 ml of PVA/PBS solution (0.5% w/v), and mixed for 30 min with a magnetic stirrer at 400 rpm (Falc Instruments mod. F60) to produce a double W/O/W emulsion. The solvent evaporation was accelerated by a continuous dropwise supply of PVA/PBS solution. Solid microparticles were filtered and washed three times with de-ionized water and stored at 4°C.

2.3 Building blocks assembly: microspheres sintering

2.3.1 Solvent-induced microspheres sintering

PCL microspheres of a selected size range (300–500, 500–630 and 630–800 μm), obtained by single emulsion, were poured into a Teflon cylindrical mould of 10 mm diameter and 4 mm height. Then, the solvent/non-solvent mixture was poured over the microspheres in 1:500 volume to weight ratio. The selected solvent/nonsolvent mixtures were composed by ethanol as non-solvent and chloroform

or dioxane as solvent. The solvent/non-solvent sintering solution was allowed to evaporate from the molded microspheres for 6 h under a chemical hood.

In a similar manner, BSA loaded microspheres and single emulsion microspheres (300–500 μm) were mixed and poured into a mould. Then, the solvent/non-solvent mixture was poured over the microspheres in 1:500 volume to weight ratio and it was allowed to evaporate from the molded microspheres for 6 h under chemical hood.

2.3.2 *Melting-induced microspheres sintering*

Melting induced microspheres sintered scaffolds were synthesized as already described in [9]. Briefly, PCL microspheres obtained by single emulsion technique, with 300–500 and 500–630 μm size range or BSA-loaded microspheres were poured into a mould and heated at 60°C in an oven (Undberg/Blue M Tube furnace) for 1 h. The scaffold obtained was then allowed to cool down to room temperature and finally was removed from the mould.

2.4 Morphological characterization

2.4.1 *Qualitative scanning electron microscope (SEM) analysis*

The morphology of the microspheres and sintered matrices was investigated by SEM (Leica 420). Samples were previously gold-coated using a sputter coater for 20 min. The BSA-rhodamine distribution inside the double emulsion microspheres was observed by confocal laser scanning microscopy (CLSM 510, Zeiss). The laser was set at 30% of full power at a wavelength of 488 nm was used as the excitation source. The spheres were viewed at the horizontal optical plain.

2.4.2 *Quantitative analysis: mercury intrusion porosimetry*

Mercury intrusion (MIP) is the experimental method used to calculate porosity features. This allows determining pore geometry and pore volume by introducing a non wetting liquid into dried scaffold under pressurized conditions (high vacuum ca. 10^{-4} torr). As pressure increases, from 400 Pa to 200 kPa, the mercury enters increasingly in smaller pores since the bigger ones. The total volume of mercury forced into the sample enables to determine the overall porosity, while the mercury volume variation measured at each pressure interval allows for the estimation of pore size using the Washburn equation [16]:

$$p \times r = -2\gamma \times \cos\theta \quad (1)$$

where p is the applied pressure, r is the radius of the pore, γ is the surface tension of the mercury and θ is the contact angle between mercury and polymer. Preliminary, the weight of the sample in the glass holder was determined both before and after the introduction of mercury. The difference in weight divided by the density of mercury at room temperature gives the total volume used. By dividing the total pore volume by the external volume of the sample, porosity or percent pore volume was determined. Finally, a built-in algorithm was used to automatically calculate pore size at each pressure interval, so that pore size distribution was obtained once all the points were recorded.

2.4.3 *Quantitative analysis: microCT*

Morphology of samples was further analyzed by using a SkyScan 1072 micro-CT desk scanner, a fan-beam scanner with a focal spot size of several microns operating up to 10 W of power. A density map of the 3D sample was depicted by absorption measurements of ionizing X-ray radiations which allows to reproduce a model of the interior of the original sample as a series of angle-by-angle sequential slices in the form of gray-scale images. Preliminary, source–detector and the source–sample distances were adequately selected to optimize the sample magnification, and thus the scan resolution. In this case, higher magnification were obtained for closer sample distance to the source and far away from the detector. Therefore, the angle-by-angle slice stack was converted in a 2D pixel maps representative of longitudinally cut slices. As output for each sample 300 serial 1,024 × 1,024 bitmap images with a resolution of 10.14 μm were obtained. Dedicated softwares (SkyScan pack–Belgium) allowed to elaborate the image stacks to re-build a 3D object. In particular, the manipulation of the grayscale thresholds enabled to finely remark the boundaries of the 3D porous scaffold, as the negative space representative of the pore volume fraction, on that characteristic parameters such as structural porosity and pore sizes were calculated. Means and standard deviations have been determined from three different 3D reconstructions for each scaffolds.

2.5 Mechanical response: compressive tests

Cylindrical samples of sintered matrices of 8 mm diameter and 4 mm height were mechanically tested in compression. Six samples for each different scaffold type were tested at room temperature using an Instron 4204 dynamometer equipped with a 1 kN load cell at a crosshead speed of 1 mm/min. Compressive modulus was calculated from the slope of the linear region of the stress–strain curves.

3 Results

Figure 1a, b shows SEM micrographs of microspheres produced by single emulsion technique with different size. The

microparticles resulted spherical and their surface appeared rough and not porous. Microstructural analysis performed by SEM and CLSM of drug-loaded microspheres prepared by double emulsion technique demonstrated that the microparticles were spherical with a porous inner structure (Fig. 1c, d). As reported in a previous work [15], the microspheres inner structure as well as protein encapsulated release kinetic could be modulated by finely varying the concentration of stabilizer (PVA) in the internal aqueous phase.

3D porous highly interconnected matrices were obtained through two different methods, the chemical and thermal assembly of protein-free microspheres obtained by single emulsion technique and protein-loaded microspheres obtained by double emulsion technique.

The former technique, named SIMS, is based on the partial dissolution of the surface of adjacent PCL microparticles. In particular, a mixture of solvents was used as solvent bath in order to dissolve the external skin of adjacent microspheres. In this case, the selected non-solvent was ethanol while the selected solvents were chloroform and dioxane.

The effect of solvent type was studied and the results are shown in Fig. 2, which depict the effect of the sintering solution chosen on the degree of sintering between microspheres. The microscopic analysis indicated that the scaffold obtained with dioxane/ethanol sintering solution (Fig. 2b, d) fused the most while those with chloroform/ethanol (Fig. 2a, c) one fused the least leading to more interconnected porous scaffold structure.

Microsphere scaffolds obtained via SIMS technique have been compared with that realized by MIMS one, based on thermal fusion of surface of adjacent microparticles. In this case, the temperature activated molecular motion of PCL chains at microsphere junction points leads to chain inter-diffusion and subsequent formation of connecting necks between microspheres [9].

The optimized processing conditions (1 h at 60°C for MIMS technique and 70/30 v/v ethanol/chloroform for SIMS technique) lead to sintered microspheres scaffolds with a well defined 3D micro-structure, as illustrated in the micrographs of Fig. 3. The microscopic analysis also indicated that microspheres are randomly packed together with connecting necks arranged uniformly along the spatial dimension. Moreover, it has been clearly identifiable on SIMS scaffolds (Fig. 3b–d), a surface porosity which is ascribable to the phase inversion process due to non-solvent addition that led to solvent removal. In particular, a higher pore density has been detected along the connection points between adjacent microspheres due to a bigger local concentration of the solvent which amplify these phenomena. SEM micrographs (Fig. 4) of matrices obtained by sintering single and double emulsion microspheres showed a uniform distribution of loaded microparticles inside the scaffold. Moreover, the loaded microspheres with smaller diameter forced a closer matrix packing leading to a decrease in the pore volume of the sintered scaffold. In particular, this effect is more remarkable in the case of MIMS technique, as the melting condition induce a higher packing degree of the microspheres.

A detailed quantitative analysis of porosity features was performed in order to quantify the effect of sintering technique and microspheres size on pore size, pore volume and

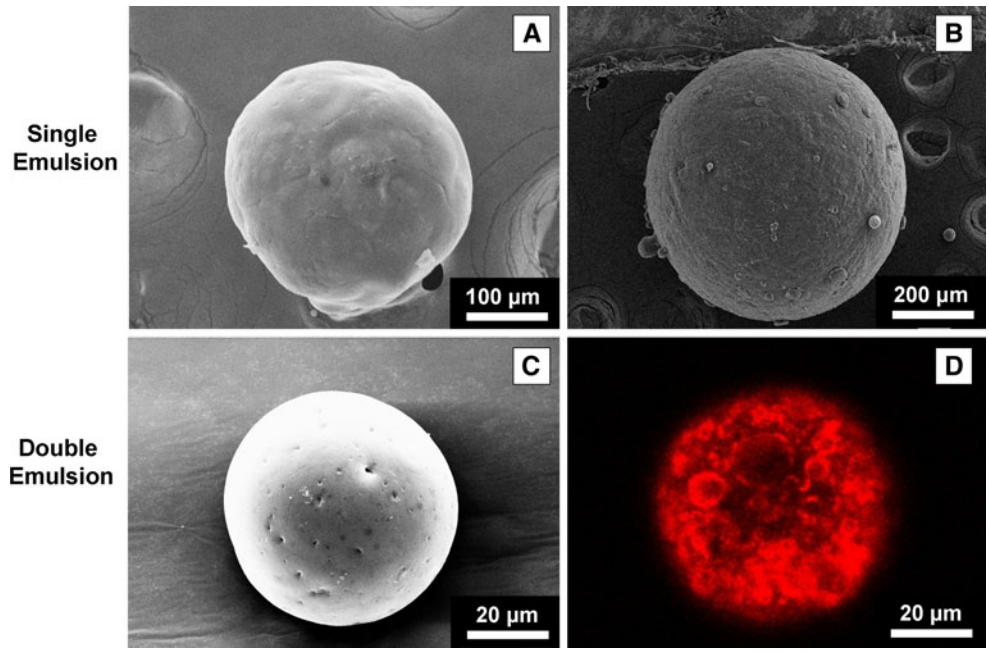

Fig. 1 SEM micrographs of PCL microparticles obtained by **a**, **b** single emulsion and **c** double emulsion. **d** CLSM image of double emulsion microspheres loaded with rhodamine-BSA

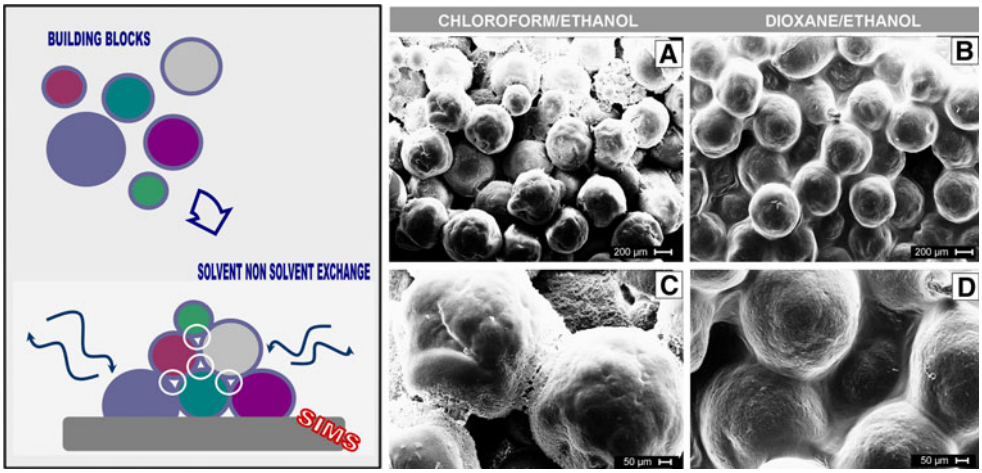

Fig. 2 SIMS scaffolds by using different binding solutions **a**, **c** ethanol/chloroform and **b**, **d** ethanol/dioxane

overall percentage of interconnected porosity of the sintered matrices. Figure 5 compares porosity data obtained by mercury intrusion porosimetry from MIMS and SIMS scaffold in order to find a relationship among microspheres size range and porosity features (i.e., pore size, pore fraction). The median pore size increased at increasing microspheres diameter range for both sintering techniques (Fig. 5). The data did not indicate any difference for the total porosity percentages of protein-free scaffolds obtained at different microspheres diameter range (about 50% for SIMS scaffold and 40% for MIMS one). SIMS scaffold showed higher total porosity percentage compared to MIMS one. Moreover, the data indicate, as expected, a decrease of total porosity percentage of SIMS and MIMS matrices obtained by sintering single and double emulsion microspheres.

The investigation of porosity features performed by microCT further confirms the indication previously obtained by mercury intrusion techniques (Fig. 6), also offering further relevant details about the scaffold morphology features. In particular, the 3D rendering of all proposed scaffolds clearly reveals a higher tendency to the structural order and homogeneity in the case of SIMS scaffolds, thus indicating a more fine control of sintering mechanism, assured by the solvent removal by controlled solvent/non-solvent exchange. Contrariwise, a drastic decay in pore sizes from (402 ± 65) to (130 ± 28) µm for MIMS scaffolds evidently remarks the "invasive" role of heating process on the microsphere morphology and, ultimately, on the pore architecture, so underlining the lacks in structural homogeneity and process resolution of MIMS technique.

Finally, the effect of sintering techniques and microspheres diameter on the compressive modulus of the sintered scaffolds was also surveyed. Figure 7a show the characteristic stress versus strain curve obtained by MIMS and SIMS scaffolds. In the small deformation range (1–10% of strain) compressive moduli of scaffolds built by microspheres with different size range were calculated. The compressive modulus increases at decreasing microspheres diameter range for both techniques. In particular, the data showed that a decrease in microspheres size range (from 500–630 to 300–500 µm) resulted in an increase in compressive modulus (from 10.1 ± 0.74 to 14.1 ± 3.4 MPa for SIMS scaffolds and from 15 ± 1.04 to 19 ± 0.96 MPa for MIMS scaffolds) (Fig. 7b). Moreover, MIMS scaffold showed higher compressive modulus compared to SIMS scaffold, in agreement with the gap in porosity previously reported.

4 Discussion

The realization of scaffolds through a bottom-up approach based on microparticles' assembly offers several advantages compared to conventional methods of porous scaffolds fabrication. In particular, it allows the independent control over pore size, interconnection, mechanical properties as well as chrono-programmed release of multiple bioactive signals. Hence, the implementation of new strategies based on the assembly of microspheres represents a basic design stage to control spatial and temporal evolution of scaffold properties, required to guide the formation of specific and complex tissues such as bone. Here, we propose two different strategies which provide the sintering of microparticles with peculiar morphological and structural properties via chemical and thermal route to engineer a synthetic scaffold that would provide a negative template for bone regeneration. Solvent induced microspheres sintering or SIMS is founded on the chemical compaction of adjacent microspheres, while melting induced microsphere sintering or MIMS, involves the thermal fusion of microspheres, produced by emulsion technique. The key factor in microspheres sintering scaffold fabrication is the control over the degree of bonding among the microspheres by finely regulating sintering conditions. A small bonding area results in weak coalescent among microspheres leading to

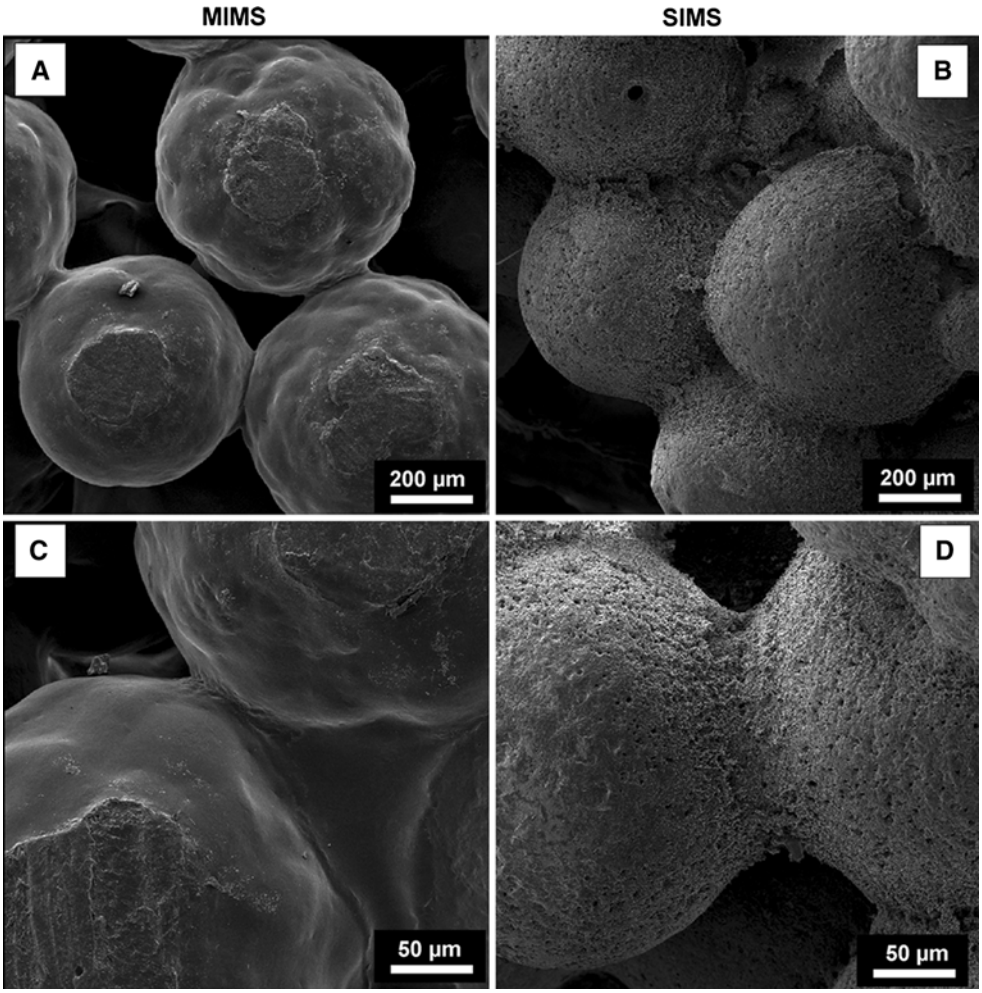

Fig. 3 SEM micrographs of 3D scaffolds obtained by **a**, **c** MIMS technique and **b**, **d** SIMS technique at different magnification

poor mechanical properties of the scaffold, while a large bonding area induces decrease in scaffold porosity and interconnection.

Referring to SIMS approach, to modulate and optimize the final properties of the scaffold, a systemic survey of the solvent mixture was undertaken to reach the correct balance between its dissolution power and evaporation kinetic. Here, chloroform and dioxane as binding agents whereas pure ethanol as non-solvent have been investigated. For both solvent/non-solvent mixtures, 80/20 v/v non-solvent/solvent ratio yielded loose packing and resulted in scaffold collapse. Contrariwise, the use of mixture composition with 60/40 v/v non-solvent/solvent ratio led to completely fused adjacent microspheres with consequent lack of pores interconnectivity (data not shown). Taking into account these limitations, the 70/30 v/v non-solvent/solvent ratio was chosen as optimal mixture composition for this particular study. Once selected the optimal solvent/non-solvent ratio, SEM micrographs of scaffolds obtained by using the ethanol/dioxane and ethanol/chloroform solution have been compared (Fig. 2). These analyses revealed that matrices obtained from ethanol/dioxane solution showed a closer matrix packing compared to scaffold obtained with ethanol/chloroform sintering solution, resulting in a decrease in the pore volume of the scaffold. This is directly ascribable to the different tendency to evaporate of solution used. Indeed, it is to be noticed that dioxane and chloroform show a boiling point of 101.8 and 61.2°C, respectively. The slower evaporation kinetic of dioxane effectively increases the binding capability of the sintering solution, so producing a more strict packing of microspheres. Moreover, weak molecules interactions among macromolecules in solution during the evaporation process also limits all mechanisms of phase separation at the microspheres' interface. This aspect has been clearly remarked in Fig. 2. The use of chloroform/ethanol as binding solution promotes an high roughness onto the microspheres surface with the formation of not homogeneous spatially distributed micropores (around 1 μ in size), due to the mechanism of phase separation. Contrariwise,

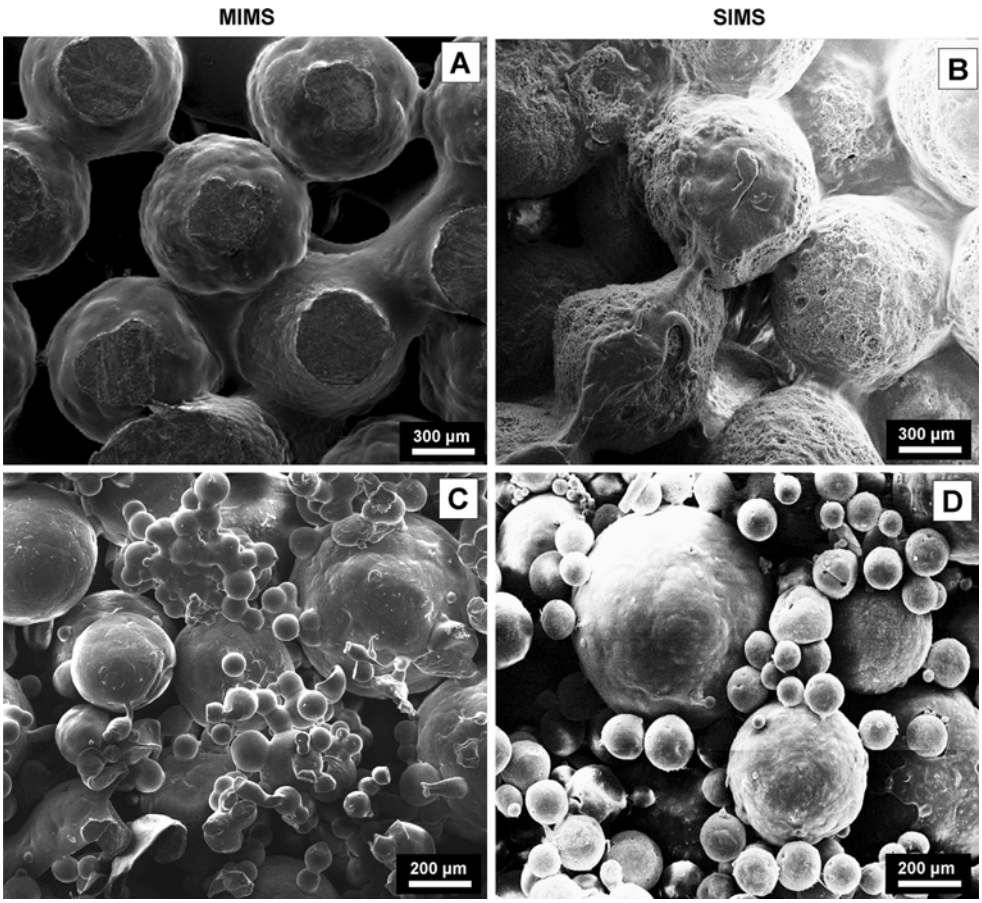

Fig. 4 SEM micrographs of MIMS and SIMS scaffolds obtained by sintering PCL microspheres produced by **a**, **b** single emulsion and **c**, **d** single and double emulsion

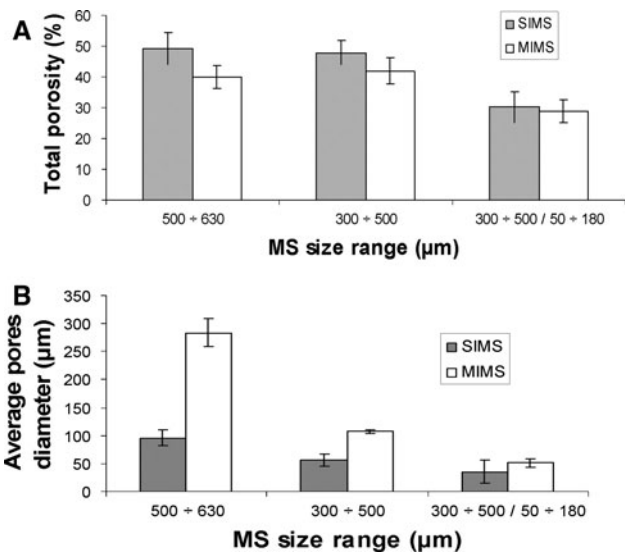

Fig. 5 Evaluation of porosity features by mercury intrusion porosimetry **a** total porosity and **b** average pore diameter of scaffolds as a function of microspheres diameter range and sintering technique

microspheres bound via dioxane/ethanol solution showed a more flat surface and pores on their surface have not been clearly detected. It implies that a fine control of phase separation drawing force may be crucial to impart a desirable surface topological properties. Indeed, it has been shown that proper surface roughness has beneficial effects on the attachment and proliferation of different cell types [17, 18].

In particular, SEM analysis of the sintered matrices obtained with ethanol/chloroform (70/30 v/v) (Fig. 3b, d) revealed a microporous surface and showed that the connecting necks among microspheres are well outlined and elongated but, at the same time, confined around the connecting points leading to a completely interconnected structure. SIMS scaffolds fabricated by sintering PCL microparticles of different size range (Fig. 4b) exhibited morphology similar to those observed with MIMS scaffold (Fig. 4a) unless additional microporosities attributed to solvent evaporation. SEM micrographs of protein loaded scaffold (Fig. 4c, d) showed that double-emulsion microspheres with smaller diameter forced a closer matrix

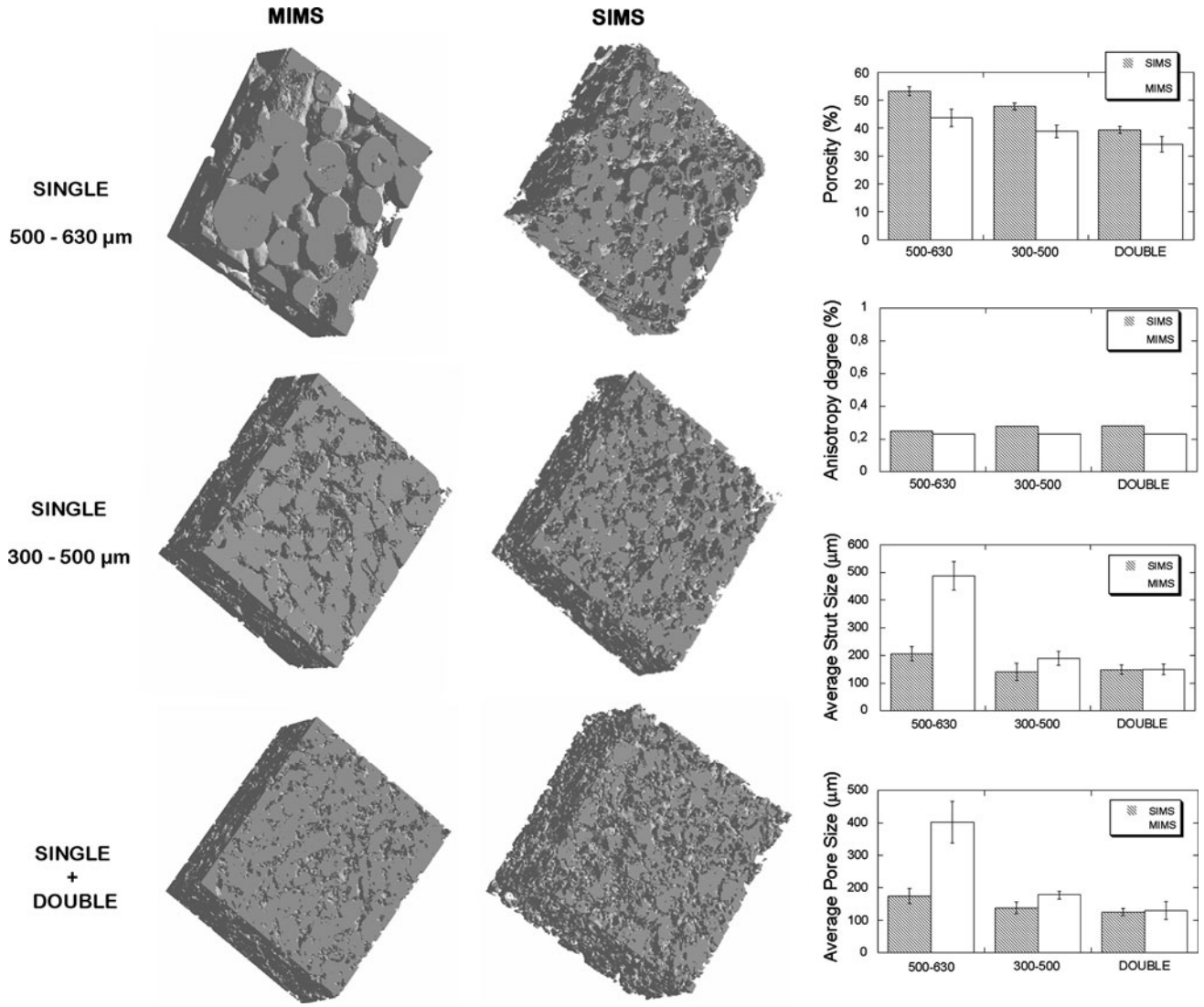

Fig. 6 MicroCT investigation on MIMS and SIMS scaffolds as a function of microspheres diameter range: 3D rendering (*left*) and quantitative evaluation of porosity features (*right*)

packing compared to single-emulsion microspheres sintered matrix resulting in a decrease in pore volume of the scaffold. In addition to SEM analysis, mercury porosimetry tests and microCT were also performed in order to compare SIMS and MIMS techniques as well as quantify the effect of building block size on porosity features of the sintered matrices, underlying the strict correlation between pores size and microspheres diameter (Figs. 5, 6). As a consequence, the proposed strategies completely satisfies the idea of bottom up approaches giving the chance to predefine the macropores size by appropriately choosing microspheres' diameter range. Interestingly the porosity percentage of the single emulsion sintered scaffold seemed to be independent on microspheres' size range for both techniques. Regardless of microspheres size, single emulsion SIMS scaffolds and single emulsion MIMS scaffolds showed a total porosity percentage of about 40 and 50% respectively (Fig. 5). The SIMS scaffolds showed a higher total porosity percentage compared to MIMS scaffolds which is thought to be caused by the additional surface porosity ascribable to solvent removal. MIP measurements on matrices obtained by sintering single and double emulsion microspheres showed that the presence of undersized microspheres tends to fill the available void spaces, so drastically reduce the total porosity of the scaffolds with a decay of about 35 and 40% for SIMS and MIMS scaffolds, respectively. However, several works demonstrated that this method largely used for studying porous materials [19], often may fails because of the application of high pressures (up to 400 MPa). This may provoke the pore structure collapse which compromises the entire scaffold architecture and therefore the measurements

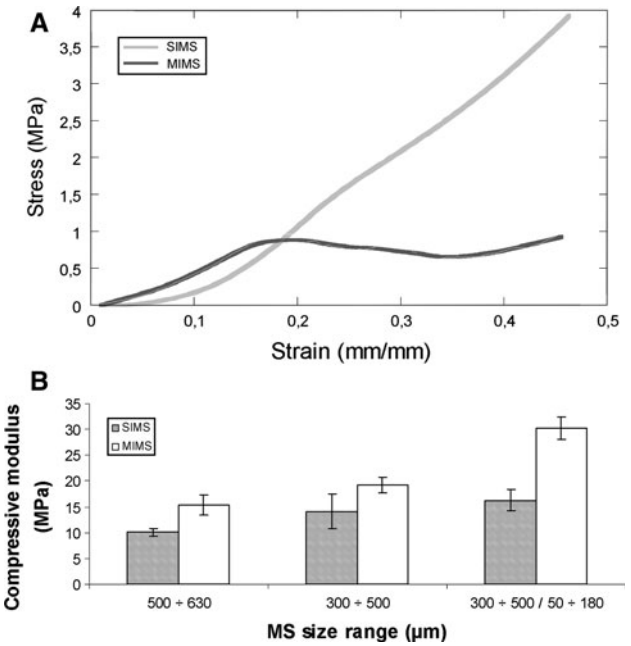

Fig. 7 Comparison of mechanical response under compression **a** representative stress versus strain curves and **b** compressive moduli of scaffolds as a function of microsphere size range and sintering technique

[20]. Moreover, this technique underestimates porosity by neglecting closed pores, since the fluid does not intrude into them, preventing a quantitative estimation of further basic structural parameters, such as pore interconnectivity, strut/wall thickness and pore anisotropy. Therefore, the adoption of optical techniques able to compute digitally images integrated with analytical procedures for the definition of morphological cues is a promising alternative approach [21].

In this work, 3D structures have been successfully investigated by a computer aided reconstruction based on microCT measurements. The use of X-ray based microtomography allows the reproduction of the complex 3D trabecular architecture of scaffolds, thus providing a direct measurements of strut/wall thickness and a visual estimation of pore size, interconnectivity, structural homogeneity and anisotropy [22]. The 3D rendering clearly reveal an evident lack in structural homogeneity in the case of MIMS scaffolds which confirms the limitation of using thermal drawing forces to control the sintering mechanism of microspheres. Contrariwise, SIMS scaffolds show pores diameter which are directly proportional to microsphere diameter, showing an average pore size ranging from (125 ± 11) to (175 ± 23) μm and an average pore strut ranging from (139 ± 17) to (206 ± 26) μm as the microspheres size increases.

Noteworthy, the results obtained by the two methods—microCT and MIP, respectively—are in good agreement, thus excluding the presence of significant population of closed pores and any mechanical failure of the scaffolds during the mercury intrusion under pressure gradient. Besides, this is also confirmed by the estimation of mechanical response by compression tests which shows elastic moduli over 15 MPa. In particular, the data showed that a decrease in microspheres size range (from 500–630 to 300–500 μm) resulted in an increase in compressive modulus (from 10.1 ± 0.74 to 14.1 ± 3.4 MPa for SIMS scaffolds and from 15 ± 1.04 to 19 ± 0.96 MPa for MIMS scaffolds) (Fig. 7). This could be ascribed to the increase of the number of connecting necks between microspheres at smaller diameters. Moreover, the addition of double emulsion microspheres and, consequently, the change in microspheres diameter range affects the mechanical response varying the compressive modulus of the sintered scaffolds. Hence, scaffolds obtained by sintering two different populations of microspheres, 300–500 and 50–180 μm range diameter respectively, exhibited the highest modulus at 16.26 ± 2.08 MPa for SIMS scaffolds and at 30.41 ± 3.24 MPa for MIMS ones. The highest modulus showed compared to single emulsion microspheres scaffolds was expected, once more, as the number of junction points should be greater. Moreover, the increase in compressive modulus at smaller microspheres diameters could be also ascribable to the decrease in total porosity of the scaffolds. However, scaffolds with mechanical properties falling in the proposed range are still reasonable for tissue engineering applications, as they are within the range of trabecular bone (0.01–2.0 GPa) as confirmed by several studies [23].

5 Conclusion

In this study, we fabricated 3D scaffolds based on SIMS. This technique provides a quick, reproducible, mild and flexible means for creating 3D scaffold and allows the independent control over pore size, interconnection, mechanical properties as well as chrono-programmed release of multiple bioactive signals. It was shown that the sintered scaffold had interconnected porous structure and mechanical properties suitable for load-bearing bone tissue engineering application. In addition, SIMS technique produces scaffolds similar to MIMS ones in terms of total porosity percentage, pore size and mechanical properties. Future study will be focused on complex tissue replacement by micropositioning the building blocks of the scaffold in order to display complex arrays of biophysical and biochemical signals following a tight dose, time and space control.

Acknowledgment This study was supported from the Ministero dell'Università e della Ricerca by funds of Rete Nazionale di Ricerca TISSUENET n. RBPR05RSM2.

References

1. Zhang S. Building from the bottom up. Mater Today. 2003;6: 20–7.
2. Ungaro F, Biondi M, d'Angelo I, Indolfi L, Quaglia F, Netti PA, La Rotonda MI. Microsphere-integrated collagen scaffolds for tissue engineering: effect of microsphere formulation and scaffold properties on protein release kinetics. J Control Release. 2006;113(2):128–36.
3. Lu HH, El-amin SF, Scott KD, et al. Three-dimensional, bioactive, biodegradable, polymer-bioactive glass composite scaffolds with improved mechanical properties support collagen synthesis and mineralization of human osteoblast-like cells in vitro. J Biomed Mater Res A. 2003;64:465–74.
4. Emily KC, Yusuf M, Laurencin CT. Amorphous hydroxyapatite-sintered polymeric scaffolds for bone tissue regeneration: physical characterization studies. J Biomed Mater Res A. 2008; 84:54–62.
5. Devin JE, Attawia MA, Laurencin CT. Three-dimensional degradable porous polymer–ceramic matrices for use in bone repair. J Biomat Sci Polym Ed. 1996;7:661–9.
6. Borden MD, Khan Y, Attawia M, et al. Tissue engineered microsphere-based matrices for bone repair: design and evaluation. Biomaterials. 2002;23:551–9.
7. Boyan BD, Hummert TW, Dean DD, Schwartz Z. Role of material surfaces in regulating bone and cartilage cell response. Biomaterials. 1996;17:137–46.
8. Borden M, El-amin SF, Attawia M, et al. Structural and human cellular assessment of a novel microsphere-based tissue engineered scaffold for bone repair. Biomaterials. 2003;24:597–609.
9. Luciani A, Coccoli V, Orsi S, Ambrosio L, Netti PA. PCL microspheres based functional scaffolds by bottom-up approach with predefined microstructural properties and release profiles. Biomaterials. 2008;29:4800–7.
10. Brown JL, Nair LS, Laurencin CT. Solvent/non-solvent sintering: a novel route to create porous microsphere scaffolds for tissue regeneration. J Biomed Mater Res B Appl Biomater. 2008;86B: 396–406.
11. Nukavarapu SP, Kumbar SG, Brown JL, et al. Polyphosphazene/nano-hydroxyapatite composite microsphere scaffolds for bone tissue engineering. Biomacromolecules. 2008;9:1818–25.
12. Zhou WY, Lee SH, Wang M, Cheung WL, et al. Selective laser sintering of porous tissue engineering scaffolds from poly(L-lactide)/carbonated hydroxyapatite nanocomposite microspheres. J Mater Sci Mater Med. 2008;19:2535–40.
13. Jaklenec A, Wan E, Murray ME, Mathiowitz E. Novel scaffolds fabricated from protein-loaded microspheres for tissue engineering. Biomaterials. 2008;29:185–92.
14. Jaklenec A, Hinckfuss A, Bilgen B, Ciombor DM, Aaron R, Mathiowitz E. Sequential release of bioactive IGF-I and TGF-b1 from PLGA microsphere-based scaffolds. Biomaterials. 2008;29: 1518–25.
15. Coccoli V, Luciani A, Orsi S, Guarino V, Causa F, Netti PA. Engineering of poly(ε-caprolactone) microcarriers to modulate protein encapsulation capability and release kinetic. J Mater Sci Mater Med. 2007;19(4):1703–11.
16. Winslow DN. Advances in experimental techniques for mercury intrusion porosimetry. In: Matjevic E, Good RJ, editors. Surface and colloid science. New York: Plenum Press; 1984. p. 259–82.
17. Borsari V, Giavaresi G, Fini M, Torricelli P, Salito A, Chiesa R, et al. Physical characterization of different-roughness titanium surfaces, with and without hydroxyapatite coating, and their effect on human osteoblast-like cells. J Biomed Mater Res B Appl Biomater. 2005;75:359–68.
18. Mustafa K, Wennerberg A, Wroblewski J, Hultenby K, Lopez BS, Arvidson K. Determining optimal surface roughness of TiO(2) blasted titanium implant material for attachment, proliferation and differentiation of cells derived from human mandibular alveolar bone. Clin Oral Implants Res. 2001;12:515–25.
19. Guarino V, Causa F, Netti PA, Ciapetti G, Pagani S, Martini D, Baldini N, Ambrosio L. The role of hydroxyapatite as solid signals on performance of PCL porous scaffolds for bone tissue regeneration. J Biomed Mat Res B Appl Biomater. 2008;86B: 548–57.
20. Ho ST, Hutmacher DW. A comparison of micro-CT with other techniques used in the characterization of scaffolds. Biomaterials. 2006;27:1362–76.
21. Guarino V, Guaccio A, Netti PA, Ambrosio L. Image processing and fractal box counting: user-assisted method for multi-scale porous scaffold characterization. J Mater Sci Mater Med. 2010;21(12):3109–18. doi:10.1007/s10856-010-4163-9.
22. Zein I, Hutmacher DW, Tan KC, Teoh SH. Fused deposition modeling of novel scaffold architectures for tissue engineering applications. Biomaterials. 2002;23(4):1169–85.
23. Keaveny TM, Hayes WC. Bone growth. In: Hall BK, editor. Bone. Boca Raton: CRC Press; 1992. p. 285–344.